Loop theory for input-output problems in cavities

H. Y. Yuan [1,2,*] Weichao Yu (余伟超) [3,4] and Jiang Xiao (萧江) [4,5,†]

[1]*Department of Physics, Southern University of Science and Technology, Shenzhen 518055, China*
[2]*Institute for Theoretical Physics, Utrecht University, 3584CC Utrecht, The Netherlands*
[3]*Institute for Materials Research, Tohoku University, Sendai 980-8577, Japan*
[4]*Department of Physics and State Key Laboratory of Surface Physics, Fudan University, Shanghai 200433, China*
[5]*Institute for Nanoelectronics Devices and Quantum Computing, Fudan University, Shanghai 200433, China*

The input-output formalism is the basis to study the response of an optical cavity to the external stimulations. The existing theories usually handle cavity systems with only one internal mode. However, there is growing interest in more complex systems, especially the hybrid cavity-matter systems, which contain at least two internal modes, one or more from both the optical cavity and the matter. Here we propose a graphical loop theory to calculate and visualize the reflection and transmission spectrum of such a multimode cavity, resembling the role of Feynman diagrams in the quantum field theory. This loop theory gives a unified picture to interpret the experimental observations of a hybrid magnet-light system and is extremely easy to apply to arbitrary complicated problems without any calculations.

I. INTRODUCTION

Exploring the nature of light and its interaction with condensed matter is a long-lasting topic in both optical and condensed-matter physics. An important knob to manipulate light is to guide it into mediums with finite volume such as cavity, waveguide, or other types of resonators. This route has inspired fruitful physical concepts, including the light quantum (photon), the squeezed state, quantum information, and numerous applications such as lasers, optical fibers, and optical tweezers. To probe the light-matter interaction, the typical practice is to put the matter in a cavity and analyze the response (the transmission and reflection probabilities) of the light modulated by the hybrid matter-cavity system. This idea has given birth to fields such as cavity quantum electrodynamics [1], cavity optomechanics [2], and cavity spintronics or spin cavitronics [3]. To interpret the reflection and transmission spectrum of light in these hybrid systems, it is essential to have a theoretical formalism to connect the input and output electromagnetic waves with the internal cavity modes. For a single-mode cavity, this relation has been well established [4–6], where the input wave stimulates the cavity mode via a Hermitian interaction, which in turn also serves as a generic decay for the cavity mode. Such a theory is sufficient to analyze the Lorentz transmission spectrum of a cavity when only one cavity mode is relevant, while the other modes are either largely detuned or not directly excited by the input wave. The situation becomes more complicated for a hybrid cavity-matter system, where the hybridized modes are close in energy and may be directly excited simultaneously. Take the cavity-magnet system as an example; the dipolar fields

produced by the precessing magnetization inevitably mix with the cavity standing wave, and it is the superposition wave that couples with the probe light [7–10]. In such situations, the traditional input-output theory is insufficient, especially when the input wave couples directly with more than one internal mode.

In this article, based on the basic principles of quantum mechanics, we propose a universal loop theory to analyze the reflection and transmission spectrum of a multimode cavity. An analytical expression of the transmission as a function of mode frequency, coupling coefficients among the cavity modes, and the dissipation strength of the cavity modes is explicitly derived. The loop theory provides an extremely simple graphical approach to solve the input-output problems in all types of cavity-based systems without carrying out tedious calculations. Because of its simplicity, the loop theory also presents a unified physical picture to understand the experimental results in different regimes, such as the asymmetric Fano resonance, Purcell effect, repulsive anticrossing in the strong-coupling regime, and the attractive level crossing in the dissipative-coupling regime.

II. PHYSICAL MODEL

We consider an n-mode cavity, as shown in Fig. 1, where the internal mode represented by operators $\hat{a}_i$ ($i = 1, 2, \ldots, n$) has natural frequencies $\omega_i = \nu_i + i\eta_i$, with ν_i and η_i being real and imaginary (dissipative) parts. These modes are not necessarily the optical modes of the cavity but can also be the modes from the matter placed in and coupled with the cavity. The cavity is connected to external ports, which guide the external wave into or out of the cavity, and the external incoming or outgoing wave is represented by operator $\hat{a}_0$, whose frequency ω can be scanned. The coupling strength between two cavity modes (modes i and j) is g_{ij}, while the

*Corresponding author: huaiyangyuan@gmail.com
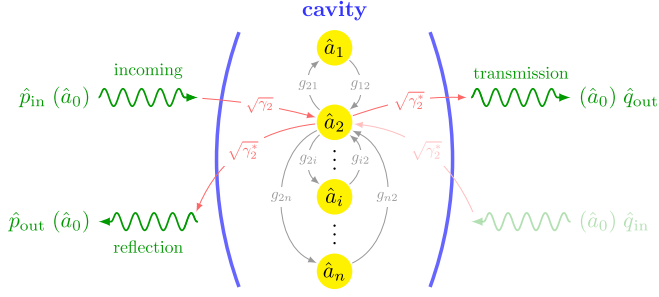†Corresponding author: xiaojiang@fudan.edu.cn

FIG. 1. A multimode cavity (modes as $\hat{a}_{1,2,\ldots,n}$) is connected with input and output via the $\hat{a}_0$ mode. The cavity modes are mutually coupled with one another via coupling strength g_{ij} and coupled with the input (output) via $\sqrt{\gamma_i}$ ($\sqrt{\gamma_i^*}$). This figure shows only the coupling connections to the $\hat{a}_2$ mode.

coupling strength between mode i and the external mode $\hat{a}_0$ is $\sqrt{\gamma_i}$. All the coupling coefficients are presumably complex. Depending on the amplitude of the coupling strength with the external mode $\sqrt{\gamma_i}$, cavities can be classified into two categories, i.e., open cavities with large openings, such as the Fabry-Pérot cavity and the cross-line cavity [11,12], and closed cavities with small openings, such as the coplanar wave guide (CPW) resonator, reentrant cavity, and rectangular cavity [13–15].

The Hamiltonian of the multimode cavity system includes the contributions from the internal cavity modes ($\hat{H}_c$), the external mode ($\hat{H}_e$), and their interactions ($\hat{H}_{int}$):

$$\hat{H} = \hat{H}_c + \hat{H}_e + \hat{H}_{int}. \tag{1}$$

Here $\hat{H}_c$ is a functional of the internal boson modes inside a cavity and their mutual interaction, i.e.,

$$\hat{H}_c = \sum_{i=1}^{n} \hbar\omega_i \hat{a}_i^\dagger \hat{a}_i + \frac{\hbar}{2} \sum_{i \neq j} (g_{ij}\hat{a}_i^\dagger \hat{a}_j + g_{ij}^* \hat{a}_i \hat{a}_j^\dagger), \tag{2}$$

where $\hat{a}_i^\dagger$ ($\hat{a}_i$) are the creation (annihilation) operators of the ith cavity mode, satisfying boson commutation relations $[\hat{a}_i, \hat{a}_j^\dagger] = \delta_{ij}$, and $g_{ji} = g_{ij}^*$ is imposed to guarantee the Hermitian nature of the system. $\hat{H}_e$ is the free Hamiltonian of the external reservoir fields,

$$\hat{H}_e = \int d\omega \, \hbar\omega \hat{a}_0^\dagger(\omega)\hat{a}_0(\omega), \tag{3}$$

where $\hat{a}_0^\dagger(\omega)$ ($\hat{a}_0(\omega)$) are the creation (annihilation) operators of the external field of frequency ω, satisfying the commutation relation $[\hat{a}_0(\omega), \hat{a}_0^\dagger(\omega')] = \delta(\omega - \omega')$. $\hat{H}_{int}$ is the interaction between the cavity modes and the external fields,

$$\hat{H}_{int} = \frac{\hbar}{\sqrt{2\pi}} \sum_i \int d\omega [\sqrt{\gamma_i^*} \, \hat{a}_i^\dagger \hat{a}_0(\omega) + \text{c.c.}], \tag{4}$$

where $\sqrt{\gamma_i}$ is the coupling amplitude between the ith cavity mode and the external field. One should note that the loop theory illustrated below holds when γ_i is frequency dependent, as long as such dependence is not too strong.
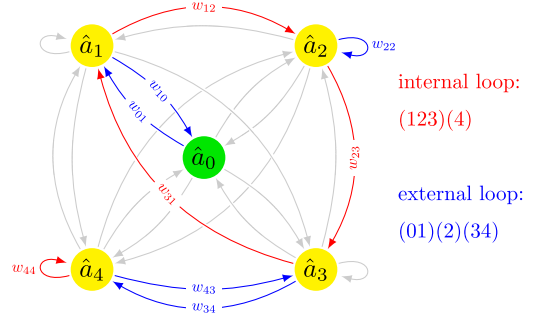

FIG. 2. The graph representation of a four-mode cavity ($n = 4$). The yellow vertices represent the cavity modes, while the green vertex represents the input or output mode. The edges connecting the vertices represent the effective coupling between the modes. The edges highlighted in red and blue represent an internal loop and an external loop, denoted as (123)(4) and (01)(2)(34).

III. THE GRAPH REPRESENTATION

To state our principle result, we first depict the multimode system as a complete *weighted directed graph* G_n with $n + 1$ vertices. An example of such a graph for $n = 4$ is shown in Fig. 2. The vertices of the graph $V(G)$ represent all the physical internal and external modes, and $E(G)$ includes all directed edges e_{ij} from $\hat{a}_i$ to $\hat{a}_j$:

$$V(G_n) = \{\hat{a}_0, \hat{a}_1, \hat{a}_2, \ldots, \hat{a}_n\}, \tag{5a}$$

$$E(G_n) = \{e_{ij} \,|\, i, j = 0, \ldots, n\}. \tag{5b}$$

The weight of the directed edge represents the effective coupling strength between the connected modes:

$$W(e_{ij}) = w_{ij} = \kappa_{ij}\sqrt{\Delta_i \Delta_j}. \tag{6}$$

Here κ_{ij} is the renormalized coupling strength defined as $\kappa_{ij} = g_{ij} - i\sqrt{\gamma_i\gamma_j^*}$ for $i \neq j \neq 0$ (note $\kappa_{ij} \neq \kappa_{ji}^*$ in general), $\kappa_{0i} = \kappa_{i0}^* = \sqrt{\gamma_i}$, $\kappa_{00} = 0$, and $\kappa_{ii} = \Delta_i^{-1} \equiv \omega_i - \omega - i\gamma_i$ represents the detuning of the cavity mode from the external input or output mode [16], and $\Delta_0 \equiv 1$.

We define an m-loop F_m as a subgraph of G_n with m vertices, and each vertex has exactly one incoming edge and one outgoing edge. Such an m-loop is, in fact, a union of disjoint cyclic paths connecting m vertices; therefore, we can use a cyclic decomposition of a permutation to represent an m-loop. For instance, for the case of $n = 4$ as depicted in Fig. 2, a 4-loop, consisting of two disjoint cycles of $\hat{a}_1 \to \hat{a}_2 \to \hat{a}_3 \to \hat{a}_1$ and $\hat{a}_4 \to \hat{a}_4$, can be represented as a permutation cycle $F_4 = (123)(4)$ or, equivalently, as (231)(4) or (312)(4). A 5-loop, formed by three disjoint cycles of $\hat{a}_1 \to \hat{a}_0 \to \hat{a}_1$, $\hat{a}_2 \to \hat{a}_2$, and $\hat{a}_3 \to \hat{a}_4 \to \hat{a}_3$, is represented as $F_5 = (01)(2)(34)$. For the purposes of this article, we are interested in only two particular types of loops: (i) the internal n-loop F_n, which involves all n cavity modes but not the external mode, i.e., $V(F_n) = \{\hat{a}_1, \ldots, \hat{a}_n\}$, and (ii) the external $(n + 1)$-loop F_{n+1}, which involves all n cavity modes and the external mode, i.e., $V(F_{n+1}) = \{\hat{a}_0, \hat{a}_1, \ldots, \hat{a}_n\}$. In general, there are $n!$ internal loops and $n \times n!$ external loops. The 4-loop (123)(4) and the
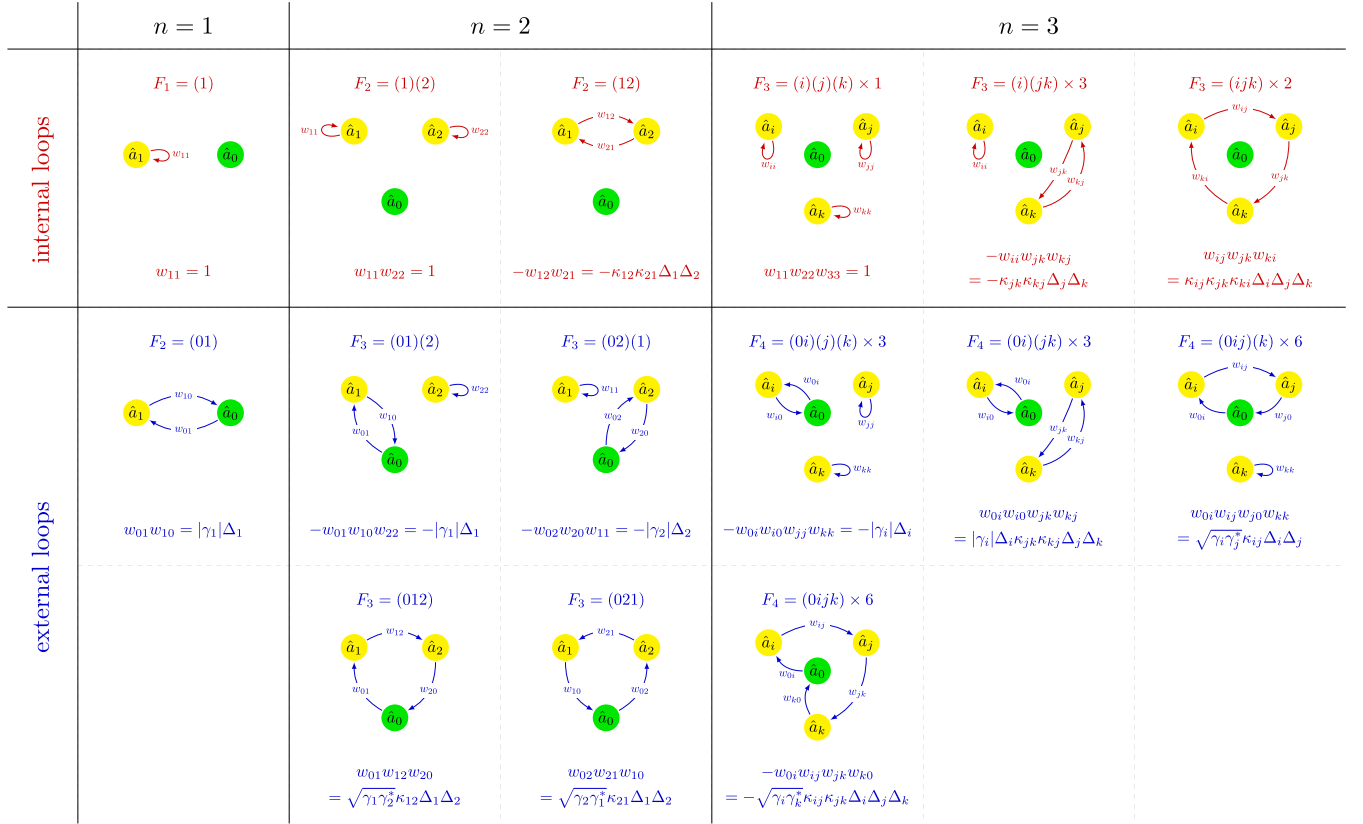
FIG. 3. All internal (in red) and external (in blue) loops for the case of $n = 1, 2, 3$. The $\mathcal{A}$ value for each loop is calculated using Eq. (7). The number following the $\times$ symbol for the $n = 3$ case indicates the number of inequivalent patterns due to different permutations of (i, j, k).

5-loop $(01)(2)(34)$ in Fig. 2 are the examples for the internal and external loops for $n = 4$.

IV. THE LOOP THEOREM

Each m-loop F_m is assigned with a dimensionless amplitude $\mathcal{A}(F_m)$ given by the product of the weight of all edges of the loop:

$$\mathcal{A}(F_m) = P(F_m) \prod_{e_{ij} \in E(F_m)} W(e_{ij}). \qquad (7)$$

Here $P(F_m) = (-1)^{m-k}$ is the parity of permutation F_m, where k is the number of disjoint cycles (brackets) of F_m.

The transmission spectrum for an open cavity system represented by graph G can be simply expressed as

$$S_{21}(G_n) = 1 + i \frac{-\sum_{\text{external}} \mathcal{A}(F_{n+1})}{\sum_{\text{internal}} \mathcal{A}(F_n)}. \qquad (8)$$

The transmission for a closed cavity is given by the same expression but with the unity removed. A detailed proof of the theorem can be found in Appendix A. The loop theorem in Eq. (8) is the central result of this article.

Physically, the sum of the amplitudes of the external loops corresponds to the superposition of different propagation channels, similar to the sum of all Feynman diagrams in a scattering process in quantum field theory. However, the internal loops in the denominator represent the renormalization from the internal scattering process.

V. APPLICATION OF THE LOOP THEOREM

Let us apply the loop theorem to study the transmission spectrum for three examples with $n = 1, 2, 3$, respectively. Based on the same rules, it is straightforward to apply the loop theorem to find the transmission for arbitrary n.

For a single-mode cavity ($n = 1$), there is only one internal (self-)loop and one external loop, as shown in Fig. 3. Plugging the corresponding $\mathcal{A}$ value for each loop from Eq. (7) in the loop theorem (8), one obtains

$$S_{21}(G_1) = 1 + i|\gamma_1|\Delta_1 = 1 + i\frac{|\gamma_1|}{\omega_1 - \omega - i\gamma_1}. \qquad (9)$$

When γ_1 is real, Eq. (9) reduces to the well-known Lorentz-type transmission spectrum for a single-mode cavity [5] with a total linewidth of $\eta_1' = \eta_1 + \gamma_1$, representing the intrinsic damping η_1 and the extrinsic damping due to leakage through the cavity ports.

For a two-mode cavity ($n = 2$), there are two internal and four external loops (see Fig. 3). Plugging the $\mathcal{A}$ value for each loop in the loop theorem (8), one obtains

$$S_{21}(G_2) = 1 + i\frac{|\gamma_1|\Delta_1 + |\gamma_2|\Delta_2}{1 - \kappa_{12}\kappa_{21}\Delta_1\Delta_2}$$
$$+ i\frac{-(\kappa_{12}\sqrt{\gamma_2^*\gamma_1} + \sqrt{\gamma_1^*\gamma_2}\kappa_{21})\Delta_1\Delta_2}{1 - \kappa_{12}\kappa_{21}\Delta_1\Delta_2}. \qquad (10)$$

This expression has parity symmetry ($1 \leftrightarrow 2$). In the most widely studied scenarios where only one out of the two internal modes is coupled to the external field, e.g., $\gamma_2 > 0$

and $\gamma_1 = 0$, Eq. (10) reduces to

$$S_{21}(G_2) = 1 - \frac{i\gamma_2}{(\omega - \omega_2 + i\gamma_2) - g_{12}^2/(\omega - \omega_1)}, \tag{11}$$

which is the widely used formula possessing the typical avoided level anticrossing feature for the two modes [9].

For a three-mode cavity ($n = 3$), there are three types (six in total) of internal loops and four types (18 in total) of external loops (see Fig. 3). By summing up all the contributions according to the loop theorem (8), one obtains

$$S_{21}(G_3) = 1 + i\frac{|\gamma_1|\Delta_1(1 - \kappa_{23}\kappa_{32}\Delta_2\Delta_3) + |\gamma_2|\Delta_2(1 - \kappa_{13}\kappa_{31}\Delta_1\Delta_3) + |\gamma_3|\Delta_3(1 - \kappa_{12}\kappa_{21}\Delta_1\Delta_2) + I}{1 - \kappa_{12}\kappa_{21}\Delta_1\Delta_2 - \kappa_{13}\kappa_{31}\Delta_1\Delta_0 - \kappa_{23}\kappa_{32}\Delta_2\Delta_3 + (\kappa_{13}\kappa_{21}\kappa_{32} + \kappa_{12}\kappa_{23}\kappa_{31})\Delta_1\Delta_2\Delta_3}. \tag{12}$$

Here

$$I \equiv -\frac{1}{2}\sum_{i\neq j}(\sqrt{\gamma_i^*\gamma_j}\kappa_{ji} + \kappa_{ij}\sqrt{\gamma_j^*\gamma_i})\Delta_i\Delta_j$$

$$+ \frac{1}{2}\sum_{i\neq j\neq k}(\kappa_{ki}\sqrt{\gamma_i^*\gamma_j}\kappa_{jk} + \kappa_{kj}\sqrt{\gamma_j^*\gamma_i}\kappa_{ik})\Delta_i\Delta_j\Delta_k$$

represents the interference effect of different scattering paths when two or more internal modes are coupled with the external wave simultaneously.

VI. PHYSICAL IMPLICATIONS

For a two-mode cavity case, when only one cavity mode ($\gamma_2 \neq 0$, $\gamma_1 = 0$) is driven by the input, the transmission can be well described by Eq. (11). Depending on the relative strength of the coupling strength g_{12} and the total dissipation of each cavity mode η_1', η_2', four types of regimes can be identified (see Appendix B for a detailed discussion): (i) the strong-coupling regime with typical avoided level crossings for $g_{12} > \eta_1'$, η_2', (ii) the asymmetric Fano line shape with electromagnetically induced transparency (EIT/MIT) at resonance for $\eta_2' > g_{12} > \eta_1'$, (iii) the Purcell regime for $\eta_2' < g_{12} < \eta_1'$, and (iv) the weak-coupling regime for $g_{12} < \eta_1'$, η_2', all of which have been demonstrated in experiments [17,18]. In fact, the seemingly simple two-mode cavity system contains much richer physics than the four well-studied regimes above. An apparent unexplored realm would be that both cavity modes are coupled to the external fields, i.e., γ_1, $\gamma_2 \neq 0$; then the interference terms [second line in Eq. (10)] will manifest. Even more versatile variants would consider the relative phase of γ_1, γ_2. All of these features are contained in the complete transmission expression (10) for a two-mode cavity obtained by the loop theorem and are yet to be explored.

An application of the three-mode cavity involves the attractive level crossing between magnon and photon modes observed in an optomagnetic cavity system by Harder *et al.* [11]. To explain the nonconventional attractive level crossing, Yu *et al.* proposed a minimal three-mode model including a magnon mode ($\hat{a}_1$), a cavity mode ($\hat{a}_2$) of low dissipation, and another hidden cavity mode ($\hat{a}_3$) of strong dissipation [10]. The transmission spectrum of such a three-mode cavity can be well captured by Eq. (12). The strong dissipation of the mode $\hat{a}_3$ simplifies the story by smearing out the interference effect, which is equivalent to neglecting the interference term $I \to 0$. Consequently, as demonstrated in Ref. [10], Eq. (12) reproduces both repulsive and attractive level crossing behaviors observed in the experiments in such systems. The core physics is that the high-dissipation mode $\hat{a}_3$, functioning as an

effective delay line for the coupling, can mediate both real and imaginary couplings between the cavity mode $\hat{a}_2$ and magnon mode $\hat{a}_1$.

The loop theorem applies to all types of coupled systems with multimode excitation, including the classical coupled oscillators, pure photonic systems [17], optomechanical systems, optomagnetic systems [7–15,18–23], and the cavity-atom system. In particular, for a cavity-atom system where an atomic state can be approximated by a two-level state, its Hamiltonian in a Jaynes-Cummings model [24] has the same form as Eq. (2) with one of the cavity modes $\hat{a}_i^\dagger$ ($\hat{a}_i$) replaced by σ^+ (σ^-), where $\sigma^\pm$ are raising (lowering) operators for the two-level state. For weak coupling or excitation, the two-level state most likely stays in its ground state such that σ^z can be replaced by its expectation value: $\sigma^z \to \langle\sigma^z\rangle \simeq -1$. This implies that the commutation relation $[\sigma^-, \sigma^+] = -\sigma^z \simeq 1$ is effectively the same as Bosonic cavity modes $[\hat{a}_i, \hat{a}_i^\dagger] = 1$. Therefore, the single-photon transmission in such a cavity-atom system [25,26] can be well captured by the loop theory without modification. There is also rising interest in the coupling or entanglement of two or more macroscopic magnets under the assistance of a single cavity mode [27,28]. Our theory provides a simple yet systematic approach in describing and understanding all these systems.

VII. CONCLUSIONS

In conclusion, we proposed a simple graphical loop theory to study the transmission spectrum of a multimode cavity. By drawing all the internal and external loops and ascertaining their amplitudes, one can obtain the analytical expressions of the reflection and transmission spectrum without much calculation.

ACKNOWLEDGMENTS

APPENDIX A: PROOF OF THE LOOP THEOREM

The Hamiltonian $\hat{H}$ leads to the following Heisenberg equation of the cavity modes and external mode:

$$\frac{d\hat{a}_i(t)}{dt} = -\frac{i}{\hbar}[\hat{a}_i, \hat{H}_c] - \frac{i}{\sqrt{2\pi}}\int d\omega \sqrt{\gamma_i^*(\omega)}\hat{b}(\omega, t), \tag{A1a}$$

$$\frac{d\hat{b}(\omega, t)}{dt} = -i\omega\hat{b}(\omega, t) - \frac{i}{\sqrt{2\pi}}\sum_i \sqrt{\gamma_i(\omega)}\hat{a}_i(t). \tag{A1b}$$

According to Eq. (A1b), the external field can be explicitly solved as

$$\hat{b}(\omega, t) = \hat{b}(\omega, 0)e^{-i\omega t}$$
$$- \frac{i}{\sqrt{2\pi}} \sum_i \sqrt{\gamma_i(\omega)} \int_0^t dt' \hat{a}_i(t') e^{-i\omega(t-t')}. \quad \text{(A2)}$$

By substituting this solution into Eq. (A1a), we obtain

$$\frac{d\hat{a}_i(t)}{dt} = -\frac{i}{\hbar}[\hat{a}_i, \hat{H}_c] - \frac{i}{\sqrt{2\pi}} \int d\omega \sqrt{\gamma_i^*(\omega)} \hat{b}(\omega, 0) e^{-i\omega t}$$
$$- \frac{1}{2\pi} \sum_j \int d\omega \sqrt{\gamma_i^*(\omega)\gamma_j(\omega)} \int_0^t dt' \hat{a}_j(t') e^{-i\omega(t-t')}.$$
$$\text{(A3)}$$

To get a Markovian quantum stochastic process, we now assume that $\gamma_i(\omega)$ is independent of frequency such that Eq. (A3) can be reduced to

$$\frac{d\hat{a}_i(t)}{dt} = -\frac{i}{\hbar}[\hat{a}_i, \hat{H}_c] + \sqrt{\gamma_i^*} \, \hat{p}_{\text{in}} - \frac{1}{2} \sum_j \sqrt{\gamma_j \gamma_i^*} \, \hat{a}_j(t),$$
$$\text{(A4)}$$

where the input field operator is defined as

$$\hat{p}_{\text{in}} = -\frac{i}{\sqrt{2\pi}} \int d\omega \hat{b}(\omega, 0) e^{-i\omega t}. \quad \text{(A5)}$$

Note that Eq. (A4) still applies when $\gamma(\omega)$ is frequency dependent, as long as the dependence is not too strong. This is because the third integral in Eq. (A3) is nearly a delta function $\delta(\omega_j - \omega)$ and the second integral can still be carried out near ω_j as long as $\gamma(\omega)$ does not have a strong frequency dependence.

According to Eq. (A4), the evolution of cavity modes at time t depends on only the information of modes at t; thus, this evolution process is Markovian. In a similar manner, we can derive the time-reversal version of Eq. (A4) as

$$\frac{d\hat{a}_i(t)}{dt} = -\frac{i}{\hbar}[\hat{a}_i, \hat{H}_c] \mp \sqrt{\gamma_i^*} \, \hat{p}_{\text{out}} + \frac{1}{2} \sum_j \sqrt{\gamma_j \gamma_i^*} \, \hat{a}_j(t),$$
$$\text{(A6)}$$

where the output field operator is defined as

$$\hat{p}_{\text{out}} = \pm \frac{i}{\sqrt{2\pi}} \int d\omega \hat{b}(\omega, 0) e^{-i\omega t}. \quad \text{(A7)}$$

Here the $\pm$ sign denotes two different definitions of the output modes [5,6], which will lead to a sign difference of $\hat{p}_{\text{out}}$ in the input-output relations.

Input-output relations

Before proceeding to a two-sided cavity, we first illustrate results for a one-sided cavity; that is, the right side of the cavity is blocked with $\hat{q}_{\text{in}} = \hat{q}_{\text{out}} = 0$ in Fig. 1 of the main text. By subtracting Eq. (A4) from Eq. (A6), the input-output relation is

$$\hat{p}_{\text{in}} - \hat{p}_{\text{out}} = \sum_j \sqrt{\gamma_j} \, \hat{a}_j. \quad \text{(A8)}$$

This relation carries the meaning that the dissipation of the cavity field equals the difference between the input and output fields. It is straightforward to generalize the input-output relation to a two-sided cavity as

$$\hat{p}_{\text{in}} - \hat{p}_{\text{out}} = \hat{q}_{\text{in}} - \hat{q}_{\text{out}} = \sum_j \sqrt{\gamma_j} \, \hat{a}_j, \quad \text{(A9)}$$

where we have assumed the coupling strengths of the input with the cavity modes through the two sides of cavity are identical. This relation is applicable to closed cavities with small openings serving as the input and output ports, such as the CPW resonator, reentrant cavity, and rectangular cavity [13–15]. For such closed cavities with small openings, the measured transmission S_{21} is defined as

$$S_{21} = \left. \frac{\hat{q}_{\text{out}}}{\hat{p}_{\text{in}}} \right|_{\hat{q}_{\text{in}}=0} = -\sum_j \sqrt{\gamma_j} \frac{\hat{a}_j}{\hat{p}_{\text{in}}}, \quad \text{(A10)}$$

and the reflection $S_{11} = 1 + S_{21}$.

For open cavities such as the Fabry-Pérot cavity and the cross-line cavity [11,12], the output $\hat{q}_{\text{out}}$ ($\hat{p}_{\text{out}}$) should be equal to the input $\hat{p}_{\text{in}}$ ($\hat{q}_{\text{in}}$) in the absence of a cavity. This requirement will modify the input-output relations as

$$\hat{p}_{\text{in}} - \hat{q}_{\text{out}} = \hat{q}_{\text{in}} - \hat{p}_{\text{out}} = \sum_j \sqrt{\gamma_j} \hat{a}_j. \quad \text{(A11)}$$

The transmission now becomes

$$S_{21} = \left. \frac{\hat{q}_{\text{out}}}{\hat{p}_{\text{in}}} \right|_{\hat{q}_{\text{in}}=0} = 1 - \sum_j \sqrt{\gamma_j} \frac{\hat{a}_j}{\hat{p}_{\text{in}}}, \quad \text{(A12)}$$

and the reflection $S_{11} = 1 + S_{21}$.

By comparing Eqs. (A10) and (A12), one immediately sees that there is an identity difference of the transmission S_{21} in these two types of cavities. In experiments, this difference will make the transmission have a peak (valley) near the resonance and be nearly equal to 0 (1) at off resonance for the closed and open cavities, respectively [11,15]. We shall focus on an open cavity with single-side input ($\hat{q}_{\text{in}} = 0$). By explicitly solving Eq. (A4) in the frequency domain, we obtain

$$\frac{\hat{\mathbf{a}}}{\hat{p}_{\text{in}}} = -i \frac{\mathbf{\Lambda}[\text{cof}\mathbf{A}]^T \cdot \mathbf{u}}{\det\{\mathbf{A}\}}, \quad \text{(A13)}$$

where $\hat{\mathbf{a}} = (\hat{a}_1, \hat{a}_2, \ldots, \hat{a}_n)^T$, $\mathbf{\Lambda} \equiv \text{diag}(\sqrt{\Delta_1}, \sqrt{\Delta_2}, \ldots, \sqrt{\Delta_n})$, $\mathbf{u} = (\sqrt{\gamma_1^* \Delta_1}, \sqrt{\gamma_2^* \Delta_2}, \ldots, \sqrt{\gamma_n^* \Delta_n})^T$, the drift matrix $\mathbf{A}$ is defined as

$$A_{ii} = 1, \quad A_{ij} = \sqrt{\Delta_i \Delta_j} \kappa_{ij}, \quad \text{(A14)}$$

and $\det\{\mathbf{A}\}$ and $\text{cof}\mathbf{A}$ are the determinant and the cofactor matrix of matrix $\mathbf{A}$, respectively. Then the transmission coefficient S_{21} with input from one side of the cavity reads

$$S_{21} = 1 - \sum_j \sqrt{\gamma_j} \frac{\hat{a}_j}{\hat{p}_{\text{in}}} = 1 + i \frac{\mathbf{v}^\dagger \cdot [\text{cof}\mathbf{A}]^T \cdot \mathbf{v}}{\det\{\mathbf{A}\}}. \quad \text{(A15)}$$

Now it is straightforward to identify the contribution of internal and external loops. (i) In the denominator, each term
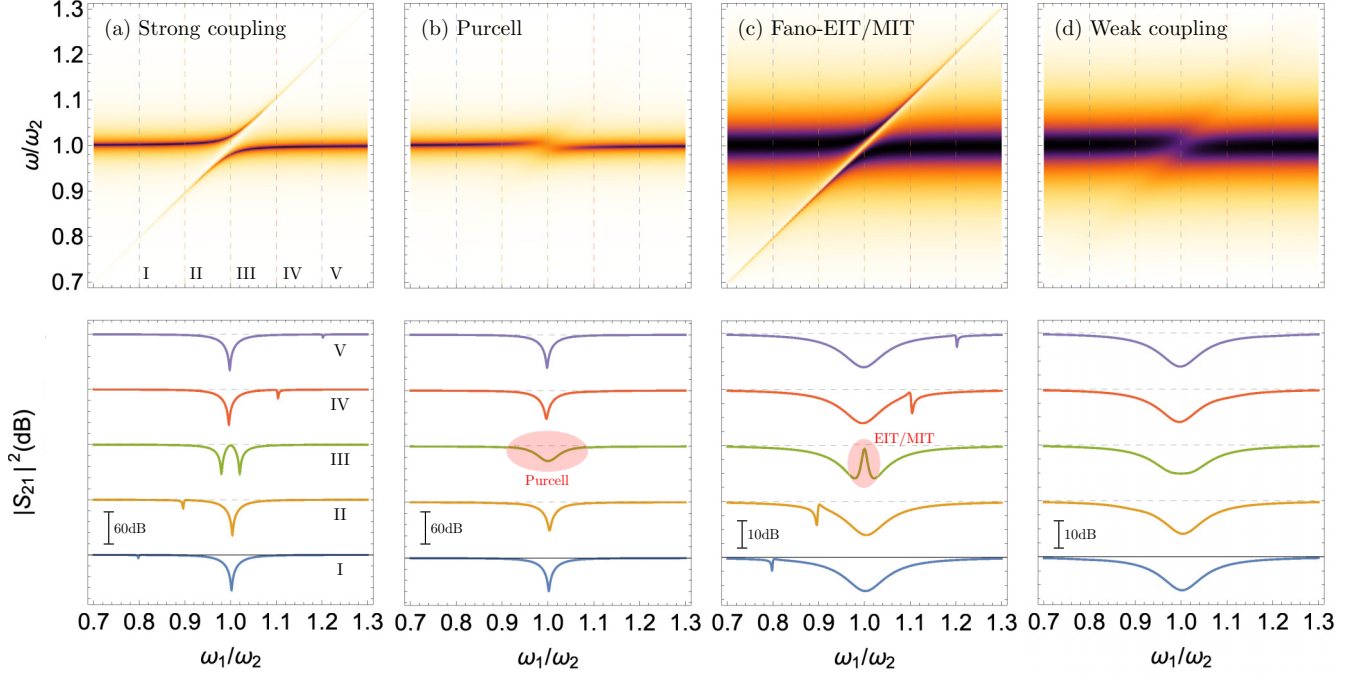
FIG. 4. Transmission spectrum of a two-mode cavity system in the (a) weak-coupling, (b) Fano-EIT, (c) Purcell, and (d) weak-coupling regimes. Parameters are (a) $\eta_1 = \eta_2 = 10^{-3}$, (b) $\eta_1 = 10^{-3}$, $\eta_2 = 0.04$, (c) $\eta_1 = 0.04$, $\eta_2 = 10^{-3}$, and (d) $\eta_1 = \eta_2 = 0.04$. The internal coupling $g_{12} = 0.02$, and external coupling $\gamma_1 = 0$, $\gamma_2 = 0.01$, $\eta_1 = \eta_2 = 2 \times 10^{-4}$. The color codes the magnitude of $|S_{21}|$ in units of dB defined as $20 \log_{10} |S_{21}|^2$. The middle panels are the transmissions at the corresponding frequencies indicated by vertical arrows. The bottom panels show the corresponding classical two-oscillator model, where the large circle has large dissipation, while the small circle has small dissipation.

in the determinant det{**A**} corresponds to a product of the weights of an internal loop running over all cavity modes $\hat{a}_1, \hat{a}_2, \ldots, \hat{a}_n$ with an overall sign given by the permutation of corresponding running order. Therefore, the denominator det{**A**} is exactly a summation of $\mathcal{A}(F_n)$ over all internal loops. (ii) In the numerator, the element (i, j) in the cofactor matrix cof**A** corresponds a product of the weights along a set of paths running through all cavity modes $\hat{a}_{1,2,\ldots,n}$ exactly once and with open ends at $\hat{a}_i$ and $\hat{a}_j$. The following multiplication with u_i^* and u_j links the two open ends with the external input mode $\hat{a}_0 = \hat{b}$, forming an external $(n+1)$-loop. Therefore, the numerator gives the summation of $\mathcal{A}(F_{n+1})$ over all external loops as promised. An overall minus sign in the numerator of Eq. (8) is because the position of the input mode $\hat{b}$ is fixed, not included in the permutation. This completes the proof of the loop theorem (8) stated in the main text.

APPENDIX B: PHASE DIAGRAM

In this Appendix, we will retrieve the four phases of a two-mode cavity system, i.e., the strong coupling with avoided level crossings, Fano effect, Purcell effect, and weak coupling. Only one cavity mode is driven by the external input; hence, the transmission should be well described by Eq. (11) of the main text.

1. Strong-coupling regime

Figure 4(a) shows the transmission spectrum of a two-mode cavity in the strong-coupling regime, $g_{12} > \gamma_i + \eta_i \equiv$

η_i'; the coupling strength is larger than the total damping γ' of cavity modes, including both the intrinsic decay and the loss from its coupling with the external input. A clear energy level anticrossing is observed near the resonance frequency (top panel), while the transmission line shapes at several ω_1 (I–V) are shown in the middle panel.

Analytically, the eigenspectrum of the two-mode Hamiltonian is

$$\omega_{\pm} = \frac{1}{2}\left[\omega_1 + \omega_2 \pm \sqrt{(\omega_1 - \omega_2)^2 + 4g_{12}^2}\right]. \quad \text{(B1)}$$

In a classical two-oscillator model, this corresponds to the driven oscillation of two coupled oscillations with coupling strength sufficiently larger than the dissipation of the oscillator [10].

2. Fano effect

Fano resonance was originally proposed by Fano to explain the asymmetric resonance line shape of helium observed in the inelastic scattering of electrons [29] and has been widely observed in atomic physics [30], plasmonic nanoparticles [31], photonic crystals [17,32], optomechanics [33], and so on. In this section, we will show that Fano-like resonance naturally appears in our multimode system. Figure 4(c) shows the transmission spectrum of a two-mode cavity system in the regime $\eta_1' < g_{12} < \eta_2'$. There are typically two resonant peaks in such a system: a symmetric one near ω_2 and an asymmetric one near ω_1. Here the asymmetric one is an example of

the Fano resonance because of the following: In general, an oscillator is in phase with the driving force below the resonance, and it has a π phase shift above resonance. For line shape II in Fig. 4(c), the natural frequencies of $\hat{a}_1$ and $\hat{a}_2$ are, respectively, $\omega_1/\omega_2 = 0.9$ and $\omega_2/\omega_2 = 1.0$. A driving force with frequency ω/ω_2 slightly larger than 0.9 will first induce an in-phase motion of $\hat{a}_2$, which further induces an out-of-phase motion of $\hat{a}_1$ through their coherent coupling. Then the out-of-phase motion of $\hat{a}_1$ acts back to $\hat{a}_2$ destructively with the original driving force on $\hat{a}_2$. A similar argument recovers a constructive interference when the driving force is slightly below $\omega/\omega_2 = 0.9$. Such an interference effect explains the asymmetric line shape of II near ω_1. One can also understand line shape IV from this logic.

The narrow peak appearing at $\omega_1 = \omega_2$ indicates the transparency of electromagnetic wave at this frequency. This is similar to the electromagnetically induced transparency (EIT) in photonics [34]. As the coupling strength of the two modes g_{12} increases, the peak height decreases and finally disappears in the strong-coupling regime ($g_{12} > \eta_2'$). The EIT-like mode can be understood as the merging of asymmetric line shapes IV and II near resonance; that is, the feedback from mode $\hat{a}_1$ to $\hat{a}_2$ is destructive to the original driving force on $\hat{a}_2$ close to the resonance. A simple mathematical view will be introduced below together with the related Purcell effect.

3. Purcell effect

Figure 4(b) shows the transmission spectrum of a two-mode cavity system in the regime $\eta_1' > g_{12} > \eta_2'$. Instead of the EIT mode observed in Fig. 4(c), a broadening of the line shape is identified near resonance. This is typically the Purcell effect [35,36], where the high dissipation mode plays as a bath to strengthen the dissipation of the low-dissipation mode. One can simply see its difference from the EIT mode from the transmission at resonance ($\omega = \mathrm{Re}\,\omega_{1,2}$):

$$
\begin{aligned}
S_{21} &= 1 - \frac{i\gamma_2}{(\omega - \omega_2 + i\gamma_2) - g_{12}^2/(\omega - \omega_1)} \\
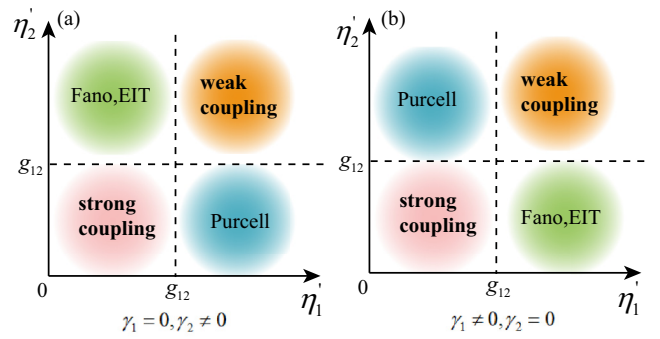&= 1 - \frac{\gamma_2}{\gamma_2' + g_{12}^2/\gamma_1'}.
\end{aligned} \tag{B2}
$$

FIG. 5. Schematic phase diagram of a two-mode system in the η_1'-η_2' plane.

When $\gamma_1' \ll g_{12} < \gamma_2'$, the second term in the denominator dominates, and it approaches infinity in the limiting case $\gamma_1' \to 0$; thus, $S_{21} \sim 1$ near resonance, i.e., the EIT mode. However, when $\gamma_1' \gg g_{12} > \gamma_2'$, the first term in the denominator dominates, while the second term enlarges the effect γ_2', and thus, $S_{21} \sim 0$ near resonance, i.e., the Purcell effect. The Purcell factor, defined as the magnitude of enhancement, can be estimated as $F_P = 1 + g_{12}^2/(\gamma_1'\gamma_2')$.

4. Weak coupling

Figure 4(c) shows the transmission spectrum of a two-mode cavity system in the regime η_1', $\eta_2' > g_{12}$. In this regime, all the interference effects are smeared out by the strong dissipation of the two modes.

Now we have shown four phases of a two-mode cavity system, including the strong coupling, Fano resonance with the EIT mode, the Purcell effect, and the weak coupling. A complete phase diagram is shown in Fig. 5(a), when the driving is on mode $\hat{a}_2$, as illustrated in Fig. 4. When the driving changes to mode $\hat{a}_1$, the positions of the EIT mode and the Purcell effect are exchanged, as shown in Fig. 5(b). These phase diagrams are universally applicable to all two-mode physical systems when only one mode is driven by or coupled to the external fields. As a demonstration of the theory, a similar phase diagram has been observed in photonics [17] and the magnet-light system [18].

[1] H. Walther, B. T. H. Varcoe, B.-G. Englert, and T. Becker, Rep. Prog. Phys. **69**, 1325 (2006).

[2] M. Aspelmeyer, T. J. Kippenberg, and F. Marquardt, Rev. Mod. Phys. **86**, 1391 (2014).

[3] D. Lachance-Quirion, Y. Tabuchi, A. Cloppe, K. Usami, and Y. Nakamura, Appl. Phys. Express **12**, 070101 (2019).

[4] M. J. Collett and C. W. Gardiner, Phys. Rev. A **30**, 1386 (1984).

[5] D. F. Walls and G. J. Milburn, *Quantum Optics*, 2nd ed. (Springer, Berlin, 2008).

[6] J. C. Garrison and R. Y. Chiao, *Quantum Optics* (Oxford University Press, New York, 2008).

[7] B. A. Auld, J. Appl. Phys. **34**, 1629 (1963).

[8] Ö. O. Soykal and M. E. Flatté, Phys. Rev. B **82**, 104413 (2010).

[9] Y. Cao, P. Yan, H. Huebl, S. T. B. Goennenwein, and G. E. W. Bauer, Phys. Rev. B **91**, 094423 (2015).

[10] W. Yu, J. Wang, H. Y. Yuan, and J. Xiao, Phys. Rev. Lett. **123**, 227201 (2019).

[11] M. Harder, Y. Yang, B. M. Yao, C. H. Yu, J. W. Rao, Y. S. Gui, R. L. Stamps, and C.-M. Hu, Phys. Rev. Lett. **121**, 137203 (2018).

[12] B. Bhoi, B. Kim, S.-H. Jang, J. Kim, J. Yang, Y.-J. Cho, and S.-K. Kim, Phys. Rev. B **99**, 134426 (2019).

[13] H. Huebl, C. W. Zollitsch, J. Lotze, F. Hocke, M. Greifenstein, A. Marx, R. Gross, and S. T. B. Goennenwein, Phys. Rev. Lett. **111**, 127003 (2013).

[14] M. Goryachev, W. G. Farr, D. L. Creedon, Y. Fan, M. Kostylev, and M. E. Tobar, Phys. Rev. Appl. **2**, 054002 (2014).

[15] L. Bai, M. Harder, Y. P. Chen, X. Fan, J. Q. Xiao, and C.-M. Hu, Phys. Rev. Lett. **114**, 227201 (2015).

[16] For a one-sided cavity with only one input and one output, one should replace γ_i by $\gamma_i/2$ in defining these coupling strengths.

[17] M. F. Limonov, M. V. Rybin, A. N. Poddubny, and Y. S. Kivshar, Nat. Photonics **11**, 543 (2017).

[18] X. Zhang, C.-L. Zou, L. Jiang, and H. X. Tang, Phys. Rev. Lett. **113**, 156401 (2014).

[19] V. L. Grigoryan, K. Shen, and K. Xia, Phys. Rev. B **98**, 024406 (2018).

[20] K. K. Chow and M. E. Hines, J. Appl. Phys. **37**, 5000 (1966).

[21] M. Weiner, J. Appl. Phys. **43**, 1246 (1972).

[22] Y.-P. Wang, G.-Q. Zhang, D. Zhang, T.-F. Li, C.-M. Hu, and J. Q. You, Phys. Rev. Lett. **120**, 057202 (2018).

[23] Y. Tabuchi, S. Ishino, T. Ishikawa, R. Yamazaki, K. Usami, and Y. Nakamura, Phys. Rev. Lett. **113**, 083603 (2014).

[24] E. T. Jaynes and F. W. Cummings, Proc. IEEE **51**, 89 (1963).

[25] S. Fan, S. E. Kocabas, and J.-T. Shen, Phys. Rev. A **82**, 063821 (2010).

[26] E. Rephaeli and S. Fan, arXiv:1208.6053.

[27] P.-C. Xu, J. W. Rao, Y. S. Gui, X. Jin, and C.-M. Hu, Phys. Rev. B **100**, 094415 (2019).

[28] F. Borjans, X. G. Croot, X. Mi, M. J. Gullans, and J. R. Petta, Nature **577**, 195 (2020).

[29] U. Fano, Phys. Rev. **124**, 1866 (1961).

[30] A. E. Miroshnichenko, S. Flach, and Y. S. Kivshar, Rev. Mod. Phys. **82**, 2257 (2010).

[31] B. Luk'yanchuk, N. I. Zheludev, S. A. Maier, N. J. Hals, P. Nordlander, H. Giessen, and C. T. Chong, Nat. Mater. **9**, 707 (2010).

[32] W. Zhou, D. Zhao, Y.-C. Shuai, H. Yang, S. Chuwongin, A. Chaha, J.-H. Seo, K. X. Wang, V. Liu, Z. Ma, and S. Fan, Prog. Quantum Electron. **38**, 1 (2014).

[33] K. Qu and G. S. Agarwal, Phys. Rev. A **87**, 063813 (2013).

[34] B. Peng, S. K. Özdemir, W. Chen, F. Nori, and L. Yang, Nat. Commun. **5**, 5082 (2014).

[35] E. M. Purcell, H. C. Torrey, and R. V. Pound, Phys. Rev. **69**, 37 (1946).

[36] E. M. Purcell, Phys. Rev. **69**, 681 (1946).